Penetration of Heavy Ions of keV Energies into Monocrystalline Tungsten

E. V. KORNELSEN
National Research Council, Ottawa, Canada

AND

F. BROWN, J. A. DAVIES, B. DOMEIJ,* AND G. R. PIERCY
Chalk River Nuclear Laboratories, Atomic Energy of Canada Limited, Chalk River, Canada

(Received 1 June 1964)

The penetration of radioactive alkali metal (Na^{24}) and inert gas (Ar^{41}, Kr^{85}, Xe^{125}, and Xe^{133}) ions into oriented monocrystals of tungsten has been measured in the energy range 0.25 to 160 keV using an electrochemical stripping technique. For energies $\leq$ 20 keV, the ion bombardments were performed in ultrahigh vacuum with the crystal surfaces free of oxides and adsorbed gases. The resulting integral penetration distributions clearly confirm the theoretically predicted channeling of the incident ions along the more open directions in the crystal lattice. Maximum channel penetrations (in the <111> and <100> directions) were observed to be about one order of magnitude larger than those measured for "amorphous tungsten." Extremely penetrating "tails" on the penetration distributions have also been observed, extending to >5 mg/cm^2 as compared to median penetrations of 0.01 to 0.2 mg/cm^2. It has been suggested to us that these are associated with excitation of the channeled atoms through multiple collisions, but definite confirmation of this mechanism has not yet been obtained.

INTRODUCTION

RECENT theoretical studies[1–3] predict that the slowing down of an energetic atomic particle in a crystalline solid can be strongly influenced by the positional correlation of the lattice atoms. In particular, atoms (or ions) incident on a crystal along the low index crystallographic directions may become focused into the open "channels" characteristic of these directions, and penetrate to a relatively great depth by a series of gentle collisions with the lattice atoms bounding the channel.

The first experimental evidence that ion penetration depths were being influenced by crystal lattice effects was obtained from range studies in polycrystalline aluminum[4] and tungsten.[5] In the measured integral range distributions in these papers a considerable fraction of the ions were found to penetrate to depths which could not be explained on the basis of a condensed gas model of the solid.[6] In comparable penetration distributions in the anodic oxides of tungsten (e.g., Ref. 5, Fig. 7) and aluminum, which are thought to be amorphous, no penetrating component was observed.

More direct experimental evidence of the channeling phenomenon has recently been obtained from measurements in monocrystalline aluminum,[7,8] tungsten,[9] copper,[10] and silicon.[11] All cases show the qualitatively predicted increase in penetration depth and its sensitivity to the orientation of the target relative to the incident ion beam.

This paper presents more detailed data on the channeling effect in tungsten, and on the previously reported[9] highly penetrating "tail" in the tungsten distributions which we believe requires a qualitively different explanation. The influences of ion energy, ion type, and crystal temperature have been explored. The experimental results proved to be very sensitive to the surface conditions of the crystal and to the alignment of the ion beam relative to the crystal axes. Since these two parameters could not be adequately controlled simultaneously (see Table I), no significance should be attached to small differences in the distributions even though the scatter of points within the individual curves was quite small.

TABLE I. Characteristics of ion bombardment facilities.

	Mass separator	uhv gun
Ion energy range	20 to 160 keV[a]	50 eV to 20 keV
Angular beam convergence	±0.6°	±0.8° for $E>1$ keV ±2.5° for $E\leq 1$ keV
Background pressure	2 to 4×10^{-6} Torr	1 to 5×10^{-10} Torr
Crystal orientation accuracy	±1°	±3°[b]
Experimental cycle time	4 h (6 to 8 crystals)	36 h (3 or 4 crystals)

[a] Using a 40-keV beam of doubly charged ions with 40-keV extra accelerating voltage on the target.
[b] Part of this error was introduced by distortion of the mounting when the crystals were heated to 2400°K for cleaning. Orientations were measured to ±1° after bombardment.

* On leave of absence from the Nobel Institute of Physics, Stockholm, Sweden.

[1] M. T. Robinson and O. S. Oen, Phys. Rev. 132, 2385 (1963).
[2] M. T. Robinson and O. S. Oen, Appl. Phys. Letters 2, 30 (1963).
[3] J. R. Beeler and D. G. Besco, J. Appl. Phys. 34, 2873 (1963).
[4] J. A. Davies, F. Brown, and M. McCargo, Can. J. Phys. 41, 829 (1963).
[5] M. McCargo, J. A. Davies, and F. Brown, Can. J. Phys. 41, 1231 (1963).
[6] O. S. Oen, D. K. Holmes, and M. T. Robinson, J. Appl. Phys. 34, 302 (1963).
[7] G. R. Piercy, F. Brown, J. A. Davies, and M. McCargo, Phys. Rev. Letters 10, 399 (1963).
[8] G. R. Piercy, M. McCargo, F. Brown, and J. A. Davies, Can. J. Phys. 42, 1116 (1964).
[9] B. Domeij, F. Brown, J. A. Davies, G. R. Piercy, and E. V. Kornelsen, Phys. Rev. Letters 12, 363 (1964).
[10] H. Lutz and R. Sizmann, Phys. Letters 5, 113 (1963).
[11] J. A. Davies, G. C. Ball, F. Brown, and B. Domeij, Can. J. Phys. 42, 1070 (1964).

EXPERIMENTAL METHOD

The experimental technique parallels closely that described in earlier papers.[5,12] Briefly, (i) tungsten monocrystal targets were bombarded along known crystal directions near normal incidence with monoenergetic beams of radioactive ions; (ii) layers of tungsten of known thickness were removed from the target surfaces by anodic oxidation followed by chemical dissolution of the oxide; (iii) the target activities were counted following each oxidation—stripping cycle. A plot of the remaining activity in the target as a function of the total thickness removed provides an integral penetration distribution of the radioactive ions in the crystal.

Bombarding Equipment

Two ion beam facilities were used to perform the radioactive ion bombardments. For energies >20 keV, the Chalk River isotope separator[4] provided the ion beams directly. For energies ≤ 20 keV, where target surface layers become more dominant, a glass envelope ultrahigh vacuum (uhv) ion gun was used.[13] This allowed the crystal surface oxide and adsorbed gases to be removed prior to bombardment. The major characteristics of the two facilities are summarized in Table I. As noted earlier, both facilities have their shortcomings. The mass separator allows fairly accurate alignment of the ion beam relative to the crystal axes ($\pm 1.6°$) but, because of the high background pressure, does not allow the crystal surfaces to be thoroughly cleaned. The uhv gun, on the other hand, permits the crystal surface to be cleaned but defines the incident angle to only $\pm 5°$.

Radioactive inert gas was supplied to the uhv gun by bombarding a vacuum-fired molybdenum strip with the appropriate ion in the mass separator, transferring the strip to the uhv system and re-evolving the gas as required by electron bombardment heating. Any chemically active gas evolved by the heating was removed by evaporated titanium getters in the uhv system.

To clean the crystals in the uhv system, each was outgassed for 20 min at 2400°K and finally flashed to the same temperature for 15 sec, 10 min before ion bombardment was begun.[14] During the final flashes, the pressure did not exceed 5×10^{-10} Torr and fell quickly toward 1×10^{-10} Torr as each crystal cooled. The time between flashing and the end of the ion bombardment was usually less than 30 min, and it is estimated that during this time less than 10% of the target surface became covered with chemisorbed gas.

[12] J. A. Davies, B. Domeij, and J. Uhler, Arkiv Fysik 24, 377 (1963).

[13] This facility will be described in a separate publication. The general techniques used have been described in detail by P. A. Redhead, E. V. Kornelsen, and J. P. Hobson, Can. J. Phys. 40, 1814 (1962).

[14] Ten minutes were required for the target to cool to within 50°K of room temperature.

Crystals

The monocrystalline tungsten was obtained from the Oak Ridge National Laboratory in the form of a rod approximately 8 mm in diameter and 150 mm long which had been grown by a modified Verneuil process involving fusion in a low-pressure arc. Its purity, by chemical analysis, was greater than 99.99%. Targets were cut from this rod by spark machining, oriented using x-ray diffraction, and heavily electropolished to remove cold work. Those to be used in the ultrahigh vacuum gun were edge-ground prior to electropolishing to obtain a uniform final size and shape (7-mm-diam disks, 2.0 mm thick). Three 0.25-mm-diam holes approximately 0.25 mm deep were ultrasonically drilled at 120° intervals in the edge of each crystal to accept tapered tungsten-mounting pins.

Four targets with surfaces approximately ($\pm 3°$) normal to each of the directions $\langle 111\rangle$, $\langle 100\rangle$, $\langle 110\rangle$, and $\langle 112\rangle$ were prepared, two of each suitable for the uhv gun. Since the ion beam was aligned with the indicated direction rather than the surface normal, the crystals are hereafter identified by this direction rather than by the exposed face whose orientation is relatively inaccurate. Four polycrystalline targets were prepared in a similar way from commercial 7.5-mm-diam tungsten rod. Back reflection x-ray patterns from this material showed no evidence of preferred orientation of the crystallites.

Electrolytic Peeling Techniques

The depth distribution of embedded radioactive atoms within each tungsten target was measured by means of the same anodizing–stripping process as was used in the earlier polycrystalline experiments.[5] This process consists of two steps: firstly, the tungsten crystal is anodized at constant voltage in a dilute HNO_3-KNO_3 solution in order to convert a known thickness of metal to WO_3 and then the WO_3 layer is dissolved in aqueous KOH. Due to the protective nature of this anodically formed oxide, extremely uniform layers of W are removed; furthermore, their thickness is uniquely determined by the applied voltage.

In order to apply the technique to monocrystalline material, it was necessary to establish what effect, if any, the orientation of the tungsten surface has on the thickness of oxide produced. Radiochemical calibrations were therefore carried out for four different orientations of tungsten $\langle 100\rangle$, $\langle 110\rangle$, $\langle 111\rangle$, $\langle 112\rangle$, using neutron-activated targets as in the previous work.[5] Within an experimental error of $\pm 3\%$ the voltage-thickness relationship was independent of orientation, except for the very thinnest films (5–20 Å). The thickness in $\mu g/cm^2$ is given by $\delta = 1.60 + 0.95\ V$ (>2.5) where V is in volts, and is reproducible to $\pm 3\%$, or 0.3 $\mu g/cm^2$, whichever is greater. Supplementary experiments suggest that, if the anodizing conditions are very care-

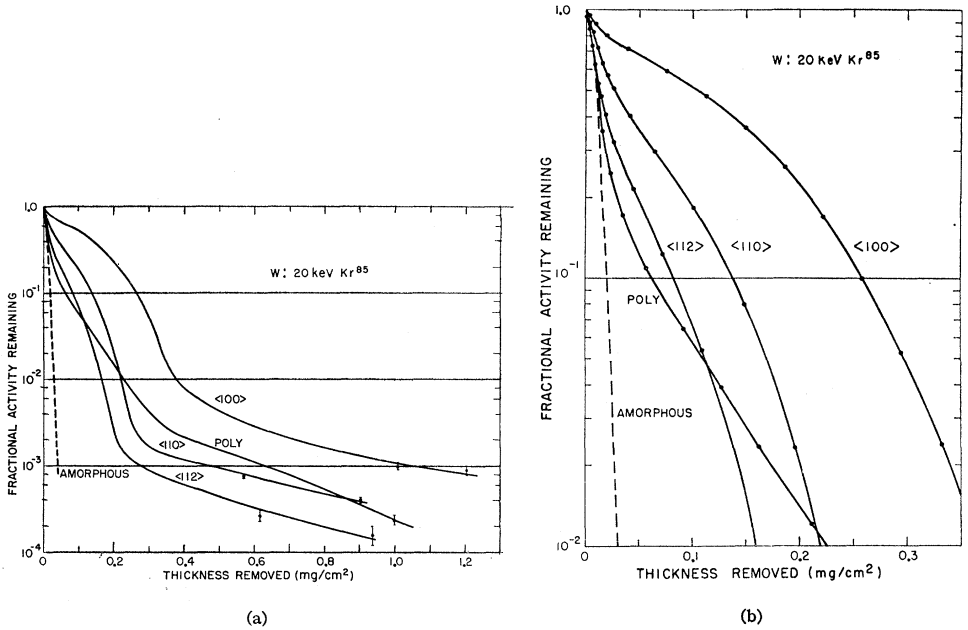

FIG. 1. (a) Integral penetration distributions for 20-keV Kr^{85} ions incident along various directions in tungsten targets. The directions indicated are approximately normal to the target surfaces. The amorphous curve was derived from penetration measurements in tungsten anodic oxide (Ref. 15). (b) The upper protion of Fig. 1(a) expanded to show the precision of data points obtained from individual anodizing–stripping cycles (filled circles).

fully controlled, this absolute limit can be reduced considerably.

Because of the extremely large penetrations observed in these monocrystalline experiments, it was sometimes necessary to remove several hundred successive layers in a single run (the maximum thickness of tungsten removable per anodizing–stripping cycle is only 75 $\mu g/cm^2$). In order to minimize the time required in such cases, the anodizing current density was increased to 50 mA/cm^2 and the concentration of the stripping solution was increased to 2%. It was thus possible to reduce the time per anodizing–stripping cycle to approximately 30 sec without significant loss of accuracy.

The counting techniques employed were identical with those reported in an earlier paper,[5] end window, flow-type, proportional β counters being used exclusively.

RESULTS AND DISCUSSION

All the data are presented in the form of integral penetration distributions, in which the remaining fraction of the original target radioactivity, which we shall refer to as "f" hereafter, is plotted on a logarithmic scale against the total weight of tungsten removed from the target surface by anodizing and stripping. Points on a distribution curve thus define the fraction of the incident beam (or more precisely that part of it which comes to rest in the target) which has penetrated to a depth *greater* than that indicated on the abscissa scale. (In tungsten, 1 $mg/cm^2 = 5220$ Å.) The curves may be differentiated to obtain concentration distributions of the radioactive atoms in the targets.

Crystallographic Direction

Distributions for ions of various energies incident on crystals of the four orientations and on polycrystalline targets are presented in Figs. 1–4. Those obtained for 20-keV Kr^{85} ions appear in Fig. 1(a) and again, on an expanded scale, in Fig. 1(b). In the latter, the experimental points from individual anodizing–stripping—counting cycles are included to illustrate the precision characteristic of most of the data. These points are omitted in Fig. 1(a) and in subsequent figures since their scatter, for $f > 3\times10^{-3}$, was usually less than the width of the graph lines. For smaller fractions, however, counting rates were low enough to give significant statistical errors. These are indicated by the bars of appropriate length (±1 standard deviation) on the figures. The curves labeled "amorphous" were derived from measured penetration distributions in the tungsten

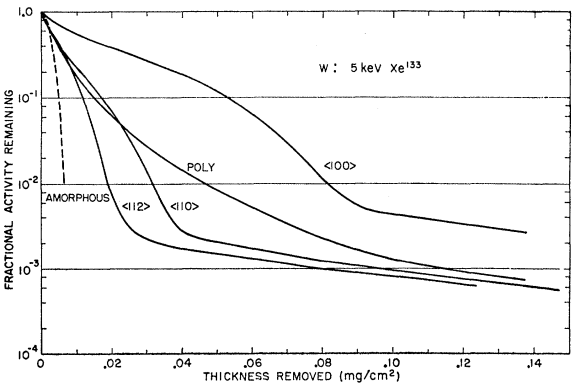

FIG. 2. Integral penetration distributions for 5-keV Xe^{133} ions in various tungsten targets.

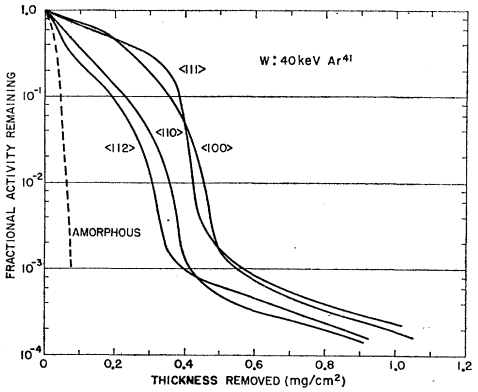

FIG. 3. Integral penetration distributions for 40-keV Ar^{41} ions in various tungsten targets.

anodic oxide WO_3, correcting approximately for the stopping power of the oxygen.[15]

The influence of crystal orientation on the ion penetration is dramatically evident in Figs. 1(a) and 1(b). The median penetrations are larger than that in the amorphous case by factors of 10.5, 2.7, and 1.3 for the ⟨100⟩, ⟨110⟩, and ⟨112⟩ directions, respectively. The depth to which 10^{-2} of the beam penetrates is, even for the least penetrating direction, (⟨112⟩), larger than the amorphous case by a factor of 5.3. The polycrystalline target distribution has a median range only slightly larger than the amorphous one, but shows an almost exponential portion similar to that observed in earlier experiments[12] involving approximately 0.15 of the particles. For $f>10^{-2}$, the distributions are qualitatively similar to those predicted for a body-centered cubic lattice by Robinson and Oen.[1] The same order of penetration depths (⟨100⟩>⟨110⟩>⟨112⟩) is also predicted by a simple "transparency model" of the lattice, but the observed depths are much too great to be accounted for by a transparency effect alone. The results thus provide firm evidence for the channel focusing mechanism they proposed.[1] A lower limit to the fraction of the ions affected by channeling should be given by that fraction penetrating beyond the maximum amorphous range (approximately 0.04 mg/cm² for 20-keV Kr^{85}). These are 0.72, 0.40, 0.24, and 0.15 for the ⟨100⟩, ⟨110⟩, ⟨112⟩ and polycrystalline cases, respectively. Inspection of Figs. 2, 3, and 4 shows that these fractions are not strongly dependent on energy or ion type. Depth distributions for polycrystalline tungsten foils given in two earlier publications[5,12] lie significantly above equivalent ones in the present paper. The implied enhancement of the channeling is thought to be a result of the cold-work introduced into the foils during rolling. X-ray and microscope examination showed that the foils used were composed of strongly oriented rather than random crystallites.

The other striking feature of Fig. 1(a) is the extremely penetrating "tail" which dominates all the distribution curves for fractions below 10^{-3}. To minimize confusion,

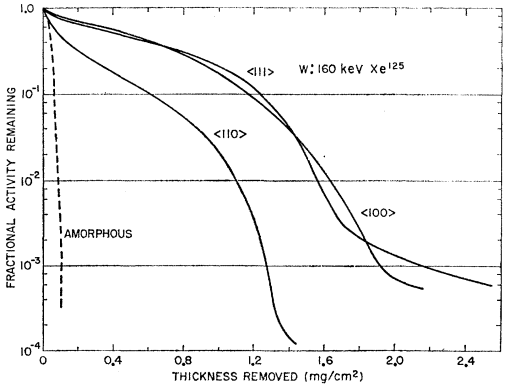

FIG. 4. Integral penetration distributions for 160-keV Xe^{125} ions in various tungsten targets.

[15] B. Domeij, F. Brown, J. A. Davies and M. McCargo, Can. J. Phys. 42, 1624 (1964).

TABLE II. Median penetrations [$R_{0.5}$ (μg/cm²)] for various bombardment parameters.

Ion	Energy (keV)	⟨111⟩	⟨100⟩	⟨110⟩	⟨112⟩	Poly	Amorphous[b]
Xe^{133}	1.0		~1.6			~1.0	
	5.0		13	3.4	3.8	3.5	
	20		77	21	9	5.9	
	20[a]	56	33	10.7	10.5		8.0
Xe^{125}	40	135	145	31	12.7	12.0	15.0
	80	195	176	55			24
	160	410	490	89			42
Kr^{85}	0.5						
	1.0		3			~1.0	
	5.0			4.6		4.7	
	20		107	27	13	11.2	
	20[a]		59.4				10.0
	40	176	145	31			19.0
Ar^{41}	40	177	170	70	44		
Na^{24}	40	377	436	95	66		39.1

[a] Mass separator bombardment.
[b] See Ref. 15.

TABLE III. Depth of penetration of 1% of ions [$R_{0.01}$ (μg/cm²)] for various bombardment parameters.

Ion	Energy (keV)	⟨111⟩	⟨100⟩	⟨110⟩	⟨112⟩	Poly	Amorphous[b]
Xe^{133}	0.5		3.0	~1.4			
	1.0		7.2	~2.0	2.8	6.0	
	5.0		81	31.7	19	46	
	20		322	185	107	138	
	20[a]	263	315	157	118		19.1
Xe^{125}	40	500	590	408	218	220	32.6
	80	915	960	670			59
	160	1558	1635	1100			93
Kr^{85}	0.5		6.3		~2.4		
	1.0		15	3.9	4.2	14.8	
	5.0			50		72.5	
	20		380	223	163	230	
	20[a]		340				30
	40	570	592	402			43
Ar^{41}	40	422	453	353	305		
Na^{24}	40	880	1100	681	618		

[a] Mass separator bombardment.
[b] See Ref. 15.

discussion of this feature will be deferred to a later section; this section will deal exclusively with the upper portion ($f>10^{-2}$) of the distributions.

Figure 2 gives distributions for 5-keV Xe^{133} ions. The abscissa scale has been expanded a factor of 10 over that of Fig. 1(a). The curves are similar in shape and ordering to those of Fig. 1(a), although the dispersion (i.e., ratio of ⟨100⟩ to ⟨112⟩ penetrations) is somewhat greater. In Figs. 3 and 4 similar sets of distributions for 40-keV A^{41} and 160-keV Xe^{125} are shown. In these cases, results for the ⟨111⟩ direction are included. Crystals of this orientation were not studied in the uhv system since their surfaces are believed to be unstable at high temperature. The triple crossing of the ⟨111⟩ and ⟨100⟩ curves has appeared in several cases. The ⟨111⟩ curve in Fig. 3 is definitely bimodal, having one concentration maximum near the surface and another near 0.4 mg/cm² depth.

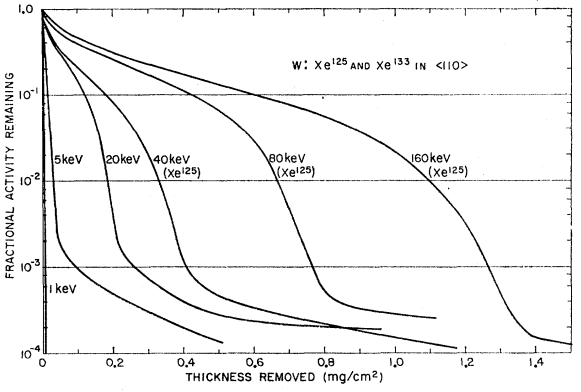

FIG. 5. Integral penetration distributions for Xe^{125} and Xe^{133} ions of various energies in ⟨110⟩ crystals.

Ion Energy

The way in which the distributions vary with incident energy for a fixed crystallographic direction is illustrated in Fig. 5 for xenon ions along ⟨110⟩. The three lowest energy curves were obtained from ultrahigh vacuum bombardments using Xe^{133}, the three highest from mass separator bombardments using Xe^{125}. The curves for $f>10^{-3}$ can be made to almost coincide by rescaling the abscissa, indicating that the fraction of the particles participating in channeling (approximately 0.5) does not vary significantly with energy. Again, in Fig. 6, the distribitions for 1-, 5-, and 20-keV Kr^{85} ions in polycrystalline tungsten follow a similar pattern. In view of the consistent shapes, the distributions can be characterized fairly well by the values of the median penetration $R_{0.5}$ and the depth required to stop all but 1% of the particles $R_{0.01}$. The latter depth can be taken as characteristic of the maximum range of the channeled particles provided the "tails" of the distributions are ignored. Tables II and III list $R_{0.5}$ and $R_{0.01}$, respectively, for most of our measured distributions, and include some values for "amorphous" tungsten for comparison.

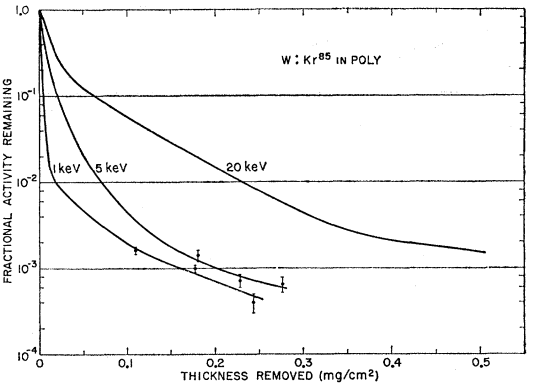

FIG. 6. Integral penetration distributions for Kr^{85} ions of three energies in polycrystalline tungsten.

The thinnest anodic oxide which can be reliably formed and stripped is ≈ 1.5 μg/cm² thick. For this reason, the values given in Tables II and III for the lowest ion energies are relatively inaccurate, being taken from distribution curves drawn through only a very few points. The extreme sharpness of the low-energy distributions is illustrated by the following example: For the 0.5-keV Xe^{133} bombardment of a ⟨110⟩ crystal, the first anodizing–stripping cycle removed 1.43 μg/cm² of tungsten and left only 0.006 of the original activity. This implies that 99.4% of the retained atoms came to

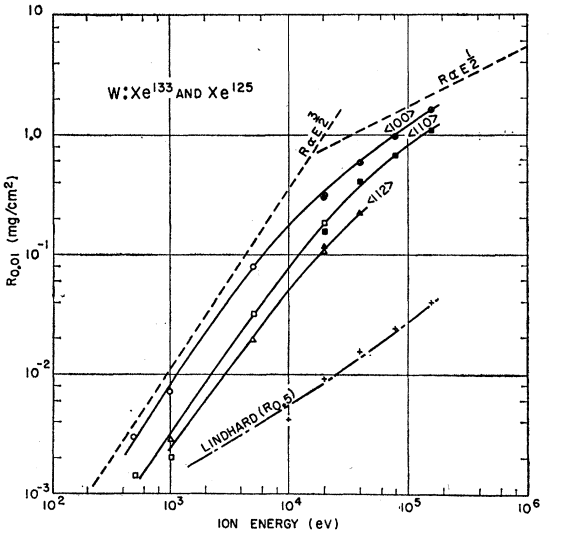

FIG. 7. The depth to which a fraction 0.01 of xenon ions penetrates along various crystal directions as a function of ion energy. Open data points are from uhv bombardments using Xe^{133}, filled points are from mass separator bombardments using Xe^{125}. The theoretical median penetration (dashed curve) was predicted (Ref. 18) on the basis of a dense gas model. The crosses are median penetrations derived from those measured in tungsten anodic oxide (Ref. 15).

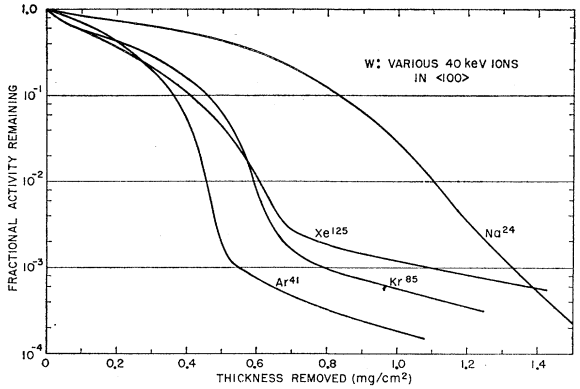

FIG. 8. Integral penetration distributions for various 40-keV ions in ⟨100⟩ crystals.

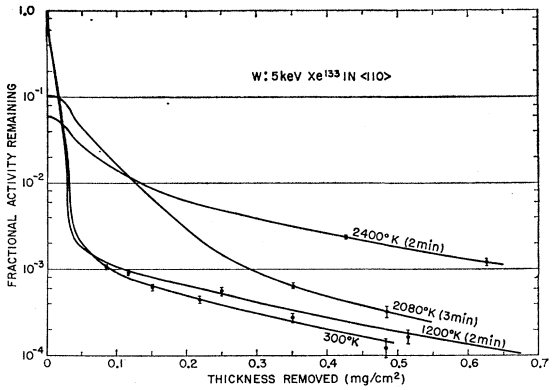

FIG. 9. Integral penetration distributions for 5-keV Xe^{133} ions in ⟨110⟩ crystals. The crystals were held at the indicated temperatures for the times shown following bombardment at 300°K.

rest in a tungsten layer approximately 7.5 Å, or less than 2.5 lattice constants thick.[16]

A logarithmic plot of $R_{0.01}$ as a function of xenon ion energy for three crystal faces appears in Fig. 7. The open experimental points were obtained from uhv bombardments, the filled ones ($\geq$20 keV) from mass separator bombardments. Curves of closely similar shape were obtained using the penetrations for $f=0.1$ rather than those for $f=0.01$ used for Fig. 7. Previously reported penetration distributions in aluminum crystals[7] also yield curves of similar shape over the investigated energy interval (20 to 160 keV).

For energies below 5 keV, the curves of Fig. 7 indicate the penetration to be proportional to $E^{1.5}$. Machine computations[17] based on purely elastic collisions of a ⟨111⟩ channeled iron atom in a bcc lattice (α iron) with initial energies 1 and 4 keV indicate a penetration dependence of the same form. This suggests that for energies below 5 keV, the energy loss is primarily by elastic collisions. For the very highest energies the curves approach the slope 0.5 which would be expected[18] from purely electronic(inelastic) energy loss. Throughout the intermediate energy region it seems likely that both types of energy loss are significant.

The median penetration of xenon in tungsten predicted by Lindhard and Scharff[19] using a "condensed gas" model of the solid, is shown by the labeled line in Fig. 7. The crosses represent experimental median penetrations in tungsten anodic oxide,[15] which is believed to be amorphous, corrected for the effect of the oxygen.

Ion Type

A comparison of the distributions for various ions of the same energy incident on ⟨100⟩ crystals is given in Fig. 8. No thorough investigation of this parameter has been attempted, and it is apparent that the behavior is not simple. From considerations of the interatomic repulsive potential alone,[20] one would expect the light ions to penetrate farther than the heavy ones. Experimentally the median ranges show this order but the $R_{0.01}$ values do not. Possibly differences in ionic size and electronic structure in addition to ion-target mass ratio contribute to the slowing-down process. More experimental data of this type are required, using a wider variety of ions.

Crystal Temperature

The effect of heating ⟨110⟩ crystals to various temperatures after bombardment at room temperature is summarized in Fig. 9. Heating to 1200°K gave no significant change in the distribution, nor decrease in the total activity (i.e., no desorption of xenon), while tempera-

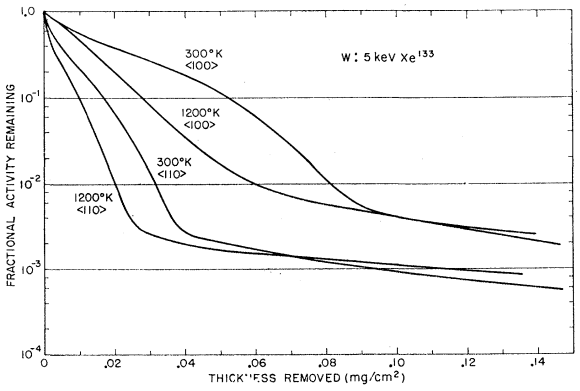

FIG. 10. Integral penetration distributions for 5-keV Xe^{133} ions in ⟨100⟩ and ⟨110⟩ crystals for bombardment temperatures of 300 and 1200°K.

[16] This result is consistent with earlier experiments involving thermal desorption of xenon from polycrystalline tungsten [E. V. Kornelsen, Can. J. Phys. 42, 364 (1964)] where it was concluded that, for ion energies <0.5 keV, the trapped xenon must be within about two lattice constants of the metal surface. In spite of the extreme proximity of the gas to the surface, the radioactivity of the bombarded crystal decreased by less than 10% upon exposure to air.

[17] C. Erginsoy (private communication).

[18] N. Bohr, Det. Kgl. Danske Videnskab. Selskab, Mat. Fys. Medd. 18, 8 (1948).

[19] J. Lindhard and M. Scharff, Phys. Rev. 124, 128 (1961).

[20] A. A. Abrahamson, Phys. Rev. 130, 693 (1963).

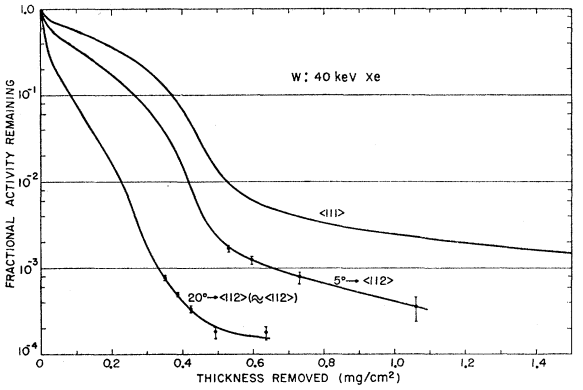

FIG. 11. Integral penetration distributions for 40-keV xenon ions in ⟨111⟩ crystals with optimum alignment and with tilts of 5 and 20° toward the ⟨112⟩ direction.

tures of 2080 and 2400°K gave progressively greater desorption and diffusive motion of the xenon in the crystal. Thus no significant diffusion of the xenon occurs for temperatures up to 1200°K.

In another experiment two crystals were held at 1200°K *during* bombardment. The predicted decrease in channeling with increasing target temperature[1] is clearly confirmed by the resulting distributions, shown in Fig. 10. The two 1200°K bombardments gave values of $R_{0.01}$ only two-thirds of those at 300°K for both the ⟨100⟩ and ⟨110⟩ crystals. Even the median penetrations are significantly reduced, particularly for the ⟨110⟩ case. As indicated above (Fig. 9), no diffusion of the xenon occurs at this temperature, and even if it did the opposite tendency would be expected.

Sensitivity of Data to Experimental Conditions

a. Misalignment

The extreme sensitivity of the distribution curves to the alignment of the ion beam with the channel direction is demonstrated in Fig. 11. Here a ⟨111⟩ crystal was bombarded, first with as accurate alignment as possible, then with deliberate tilts of 5° and 20° toward a ⟨112⟩ direction. Even the 5° tilt reduces the median penetration from 0.130 to 0.045 mg/cm²; almost a factor of 3. The distribution for the 20° tilt, which almost coincides with a ⟨112⟩ direction, has both $R_{0.5}$ (0.013) and $R_{0.01}$ (0.223) characteristics of the ⟨112⟩ crystal bombardment (see Tables II and III).

b. Surface Contamination

Surface oxide layers and/or adsorbed gases also strongly affect the distributions. In Table II, the median ⟨100⟩ penetrations for 20-keV Xe^{133} and Kr^{85}, from the uhv bombardments, are about twice the values obtained from the mass separator bombardments. The corresponding values of $R_{0.01}$ (see Table III) differ relatively little. Errors in crystal alignment, which are on the average larger in the uhv system, would tend to give the opposite effect. A third 20-keV Kr^{85} bombardment was performed on a ⟨100⟩ crystal on which 3 μg/cm² (approximately 16 Å) of tungsten was first converted to anodic oxide. Figure 12 shows the resulting distribution compared with those from the uhv and mass separator bombardments. The thin oxide layer, which transmits about 80% of the ions, has reduced the channeling to even less than was observed for the polycrystalline target [see Fig. 1(a)]. The ions thus appear to undergo a strong dispersion in direction in traversing the oxide. The difference between the uhv and mass separator distributions might be explained by a similar dispersion in only a few atom layers of surface oxide or adsorbed gas.

c. Radiation Damage

Most of the distributions were obtained with bombardments of less than 2×10^{13} ions/cm² to avoid possible

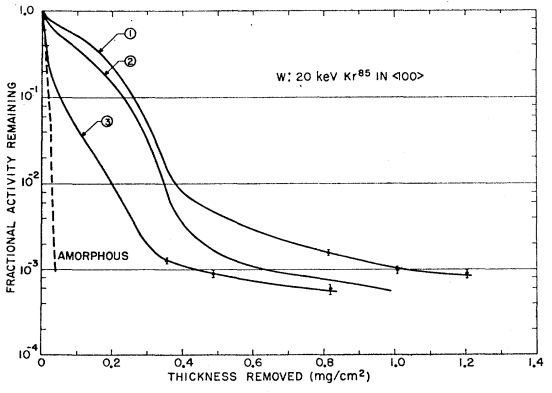

FIG. 12. Integral penetration distributions for 20-keV Kr^{85} ions in ⟨100⟩ crystals showing the effect of crystal surface conditions: curve (1) uhv bombardment of a clean crystal; curve (2) mass separator bombardment; curve (3) mass separator bombardment of a crystal with 3 μg/cm² of tungsten converted to anodic oxide.

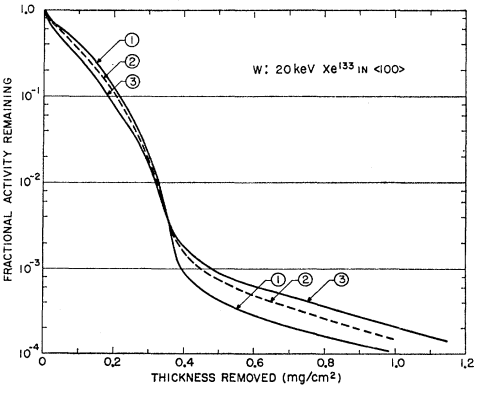

FIG. 13. Integral penetration distributions for 20-keV Xe^{133} ions in ⟨100⟩ crystals showing the effect of prior ion bombardment: curve (1) uhv bombardment of a clean, unbombarded crystal; curve (2) uhv bombardment of a clean crystal previously bombarded with 5×10^{14}/cm² 5-keV natural xenon ions; curve (3) mass separator bombardment.

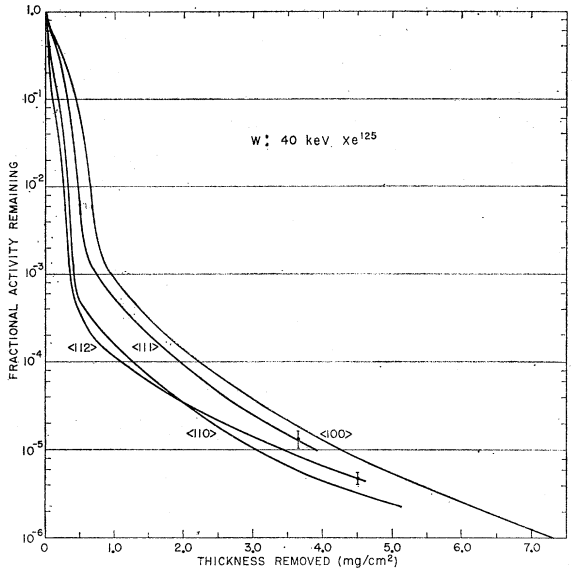

FIG. 14. Integral penetration distributions for 40-keV Xe^{125} ions in various crystals extended to greater depths to show the parallelism of the tails.

interaction between incoming ions and those already brought to rest.[16] In Fig. 13 is shown the effect of deliberately prebombarding a ⟨100⟩ crystal with approximately 5×10^{14}/cm² of 5-keV natural xenon ions; i.e., about half the number of atoms in a tungsten monolayer. According to radiation damage calculations,[21] such a bombardment should produce a large number of vacancy-interstitial pairs in a layer of thickness comparable to the penetration depth (in this case $R_{0.01}=0.08$ mg/cm²). Even if only one vacancy-interstitial pair were created per incident ion (undoubtedly an underestimate) a large fraction of the channels should be affected if the defects were stable. The distribution curve (curve 2 of Fig. 13), however, lies only slightly below that for the normal uhv bombardment (curve 1) and in fact lies above the mass separator case (curve 3). The fraction of the 20-keV ions penetrating through the "disturbed" region is reduced by only about 20% (from 0.45 to 0.37) and at lower fractions the curves converge again. The implication is very strong that most of the damage produced by the ions quickly anneals out at room temperature.

The Penetrating Tails of the Distributions

Let us now examine in more detail the extremely penetrating "tails" which appear on nearly all of the integral penetration distributions. To illustrate the phenomenon more clearly, distributions obtained from higher intensity 40-keV Xe^{125} bombardments of four crystals are shown in Fig. 14. Up to penetration depths of several microns, the tails of the four curves remain nearly parallel, and tend to decrease in slope rather than having the downward curvature expected near a maximum range.

An experiment was performed to provide evidence that the tails are not the result of incomplete anodizing or stripping of the crystal surface. A ⟨100⟩ crystal was anodized to a voltage converting 9 μg/cm² of tungsten to oxide and was then bombarded with 2-keV Xe^{133} ions in the mass separator. The resulting depth distribution showed no tail within two orders of magnitude of the level expected from bombardment of a clean ⟨100⟩ crystal. This demonstrates that the entire surface of the crystal does indeed become oxidized and that the oxide is completely dissolved.

Two auxiliary experiments confirm that the particles have, in fact, penetrated to the depths indicated and that the tails are not an experimental artifact.

(a) For one of the high-intensity bombardments of Fig. 14, the channeling portion of the distribution (i.e., a depth of about 1.0 mg/cm²) was first removed. The conversion electron spectrum of the remaining Xe^{125} was then measured in a high-resolution β spectrometer.[22] Comparison of the K_{55} and K_{188} conversion lines with those from previous calibration runs[23] indicated an average depth of the embedded Xe^{125} of 0.5 mg/cm², in good agreement with the half-widths of the tails in Fig. 14.

(b) Simultaneous β and γ counting during various stages of peeling of another of the high-intensity runs again showed, by reduction of the β counts relative to the γ, that the average depth of the embedded Xe^{125} in the tails was approximately 0.5 mg/cm². This method is described more fully in Ref. 9.

The figures of the present paper show that, with the exception of the polycrystalline targets, the slope of the tail at a given depth is independent of ion energy, crystal direction, temperature, and ion type, within experimental error. The fraction of the ions contributing to the tails, on the other hand, varies by almost two orders of magnitude. It is suggested that the slope must be determined by some bulk property common to all the crystals, such as the equilibrium defect or impurity density; while the fraction of the particles involved depends on the bombardment parameters.

Differences of less than a factor of two are probably not significant because of the high sensitivity to misalignment which can be seen in Fig. 11. Tails such as those seen in Fig. 13, and the ⟨110⟩ and ⟨112⟩ cases of Fig. 2, for example, should be considered the same within experimental error.

There is a general tendency [see Figs. 1(a) and 2] for the crystal directions showing the greatest channeling to have the highest fraction of particles in the tail. Also,

[21] J. B. Gibson, A. N. Goland, M. Milgram, and G. H. Vineyard, Phys. Rev. 120, 1229 (1960).

[22] R. L. Graham, G. T. Ewan, and J. S. Geiger, Nucl. Instr. Methods 9, 245 (1960).

[23] R. L. Graham, F. Brown, J. A. Davies, and J. P. S. Pringle, Can. J. Phys. 41, 1686 (1963).

as in Fig. 8, the ion types (Na^{24} excepted) showing the greatest maximum range have the highest tail fraction.

For a given crystal direction (see Fig. 5) the tail at any specified depth tends to lie lower with decreasing incident ion energy. The only distributions for which no tails were observed were those at the very lowest energies such as the 1-keV Xe^{133} in ⟨110⟩ seen in Fig. 5. Other examples were the 0.25-keV Kr^{85} bombardments of ⟨110⟩ and ⟨112⟩, 0.5-keV Xe^{133} in ⟨112⟩, ⟨110⟩, and ⟨100⟩. The 1-keV bombardments of ⟨100⟩ crystals, however, showed definite tails both for Kr^{85} and Xe^{133}.

The tail fraction appears (see Fig. 10) to be completely independent of the crystal temperature during bombardment, and also to post-bombardment heating (Fig. 9), except for temperatures greater than 1200°K where diffusion and desorption of the trapped gas are taking place.

The surface condition of the crystal, which plays an important part in the channeling phenomenon has a relatively minor effect on the tail fraction (Fig. 13), while the prebombardment of the target shown in Fig. 14 has no significant influence at all.

The physical mechanism responsible for the penetrating tails has not yet been definitely established. It seems unlikely that ordinary diffusion can be playing a significant part, in view of the temperature independence and the small fraction of the particles participating. The possibility of some special type of diffusion involving particles in anomalous (excited) states or traversing anomalous regions of the crystals such as dislocation lines also seems improbable; such a mechanism should not show the extreme dependence on crystal alignment illustrated in Fig. 11. The latter evidence, in fact, suggests that the effect is a dynamic one, taking place in the channels before the particles have come to thermal equilibrium with the lattice. An alternative possibility is the interstitial diffusion of particles which, by being perfectly channeled, have lost their energy without producing atomic displacements. Their diffusive motion would stop when they encountered a vacancy.

Macroscopic cavities in the crystals in which the anodizing or stripping operations were ineffective could, in principle, be responsible for the tails, but they would have to have dimensions comparable with the maximum penetration (several microns) normal to each crystal surface, and much smaller dimensions in the transverse direction to give the alignment sensitivity. The existence of such cavities in all the crystals and in the polycrystalline material as well seems unlikely. Electron micrographs of the crystal surfaces with resolution of approximately 50 Å showed no feature which could be interpreted as cavities.

From the maximum penetration observed for 1-keV ions (above 5 mg/cm^2) the rate of energy loss in the tails can be as low as a few hundredths of an electron volt per angstrom. This is to be contrasted with a minimum rate in the "ordinary channeling" (see Fig. 7) of about ten electron volts per angstrom unit. Such a low rate of energy loss is inconsistent with any realistic interatomic potential between neutral atoms. The independence of the tail on crystal temperature, in contrast with the strong dependence of channeling on temperature (Fig. 10) also suggests that normal collisions involving the bounding atoms of the channels do not dominate the energy loss.

An interesting mechanism which accounts for the major observed features of the tails has been suggested by Erginsoy in a recent letter.[24] He suggests that the channeled atoms may undergo collisional excitation in a series of inelastic collisions, and attain a state in which they are able to travel down the channels with extremely low rates of energy loss. He proposes that the major stopping mechanism is encounters with lattice defects which bring individual particles rather abruptly to rest, rather than a gradual slowing down of the particle in the channel.

Such a theoretical description has several attractive features. In particular, the slope of the tail would then be determined by the bulk defect or impurity density of the crystals. The greater slopes observed for the polycrystalline case would then imply a greater density of "stopping centers" in this material. The sensitivity to crystal alignment could be interpreted as varying the fraction of particles sufficiently well directed to avoid large-angle collisions at the channel boundaries over distances longer than the average distance between defects.

Perhaps the greatest weakness of this proposal is that it does not, at present, indicate why tails are observed in tungsten crystals but not in aluminum[7,8] or in silicon.[11] It should be noted, however, that the depth distributions for the latter cases were followed only to $f=10^{-4}$, and the possible existence of tails at lower levels cannot be excluded.

CONCLUSIONS

The experimental data provide firm qualitative support for the channeling phenomenon in tungsten. Approximate values of maximum channel penetration and fraction of atoms channeled have been obtained for various crystallographic directions and ion energies. More precise quantitative data would require improved ion beam alignment and control of the target surface conditions simultaneously. The observed temperature effects agree qualitatively with those predicted. They are sufficiently large that collision calculations will require explicit account of the crystal temperature before meaningful comparisons can be made with experimental data.

The penetrating tails of the integral penetration distributions have tentatively been assigned to inelastic collision effects taking place among the channeled atoms possibly leading to their autoionization. No critical test of this postulate has, however, yet been made.

[24] C. Erginsoy, Phys. Rev. Letters 12, 366 (1964).

ACKNOWLEDGMENTS

The authors are indebted to Atomic Energy of Canada Limited, the National Research Council of Canada, and the Nobel Institute of Physics, Stockholm, for the opportunity to assemble the cooperative program which led to the results presented in this paper. The contributions of the technical group of the Electron Physics Section, National Research Council, who constructed the ultrahigh vacuum system, and of the mass separator group of the Research Chemistry Branch, Atomic Energy of Canada Limited, are gratefully acknowledged.

We benefited greatly from discussions with M. T. Robinson and O. S. Oen of the Oak Ridge National Laboratory, and with C. Erginsoy of Brookhaven National Laboratories.

PHYSICAL REVIEW VOLUME 136, NUMBER 3A 2 NOVEMBER 1964

Shubnikov–de Haas Effect and Cyclotron Resonance in a Dilute Bi-Sb Alloy

YI-HAN KAO,*R. D. BROWN, III, AND R. L. HARTMAN
IBM Watson Laboratory, Columbia University, New York, New York
(Received 11 May 1964)

Magnetoresistance oscillations (Shubnikov–de Haas effect) and Azbel-Kaner cyclotron resonance were studied in a dilute Bi-Sb alloy (Sb concentration of 0.96 wt. %) at 4.2°K for various orientations of the magnetic field. It was found that the electron cyclotron masses, and the extremal cross-sectional areas of the electron Fermi surface, decrease to approximately 80 and 62%, respectively, of the corresponding values in pure Bi. The observed changes in cyclotron masses and Shubnikov–de Haas frequencies in the alloys are consistent with the nonparabolic model and the assumption of rigid motion of the conduction band, and the valence band just beneath it, with respect to the hole band. Effective masses at the bottom of the conduction band were calculated. The electron Fermi energy and concentration in the alloy were determined. The band overlap deduced from this result is in agreement with other work.

I. INTRODUCTION

THE Shubnikov–de Haas effect and Azbel-Kaner cyclotron resonance have been used to investigate the electronic band structures of pure Bi and Sb. These are semimetals characterized by low Fermi energies and charge carriers (electrons and holes in equal number) of small momentum. It is plausible, because of the long de Broglie wavelength of the charge carriers at the Fermi energy in Bi, that the local perturbation produced by alloying a small amount of Sb in Bi will not be resolved and the mean free path of the charge carriers will not be substantially decreased. This argument, as well as the results of Esaki and Heer,[1] suggest that it will be feasible to observe the Shubnikov–de Haas effect and cyclotron resonance in dilute Bi-Sb alloys, and to study their electronic band structure by these effects. The present work reports the observation of these effects in a 1% alloy and gives information on the band structure of dilute Bi-Sb alloys. To the best of our knowledge, the Shubnikov–de Haas effect and Azbel-Kaner cyclotron resonance have not been observed in Bi-Sb alloys in the past.

Bi and Sb are group V elements and have very similar crystalline structure. X-ray studies[2] have shown that alloying Bi and Sb results in changes in the lattice parameters. The addition of (neutral) Sb to a Bi crystal can then be expected to alter the energy band structure and change the electron and hole concentrations by equal amounts. De Haas–van Alphen studies[3,4] reveal that the extremal cross-sectional areas of the electron Fermi surface and the Fermi energy in pure Bi decrease with increasing Sb concentration; i.e., that the overlap of the conduction and valence band decreases with alloying.

Theoretical and experimental studies[5–7] have shown that the conduction band in Bi is nonparabolic. According to this model, the cyclotron masses change when the Fermi energy is decreased by alloying with Sb. In our experiments, we observed this change of cyclotron masses of electrons directly. These data, together with the Shubnikov–de Haas data, are consistent with the nonparabolicity to be associated with a gap between the conduction band and the (lower) valence band of ~15 meV and a rigid motion, upon alloying, of these bands with respect to the hole band. It should be

* Present address: Department of Physics, State University of New York, Stony Brook, Long Island, New York.
[1] L. Esaki and J. Heer, J. Appl. Phys. **34**, 234 (1963).
[2] P. Cucka and C. S. Barrett, Acta Cryst. **15**, 865 (1962).
[3] D. Shoenberg and M. Zakki Uddin, Proc. Roy. Soc. (London) **A156**, 687 (1936).
[4] N. B. Brandt and V. V. Shchekochikhina, Zh. Eksperim. i Teor. Fiz. **41**, 1412 (1961) [English transl.: Soviet Phys.—JETP **14**, 1008 (1962)].
[5] B. Lax, Bull. Am. Phys. Soc. **5**, 167 (1960); B. Lax, J. G. Mavroides, H. J. Zeiger, and R. J. Keyes, Phys. Rev. Letters **5**, 214 (1960).
[6] M. H. Cohen, Phys. Rev. **121**, 387 (1961).
[7] R. N. Brown, J. G. Mavroides, and B. Lax, Phys. Rev. **129**, 2055 (1963).